PERFORMANCE IMPROVEMENT OF A COUNTER-FLOWING DOUBLE-PIPE HEAT EXCHANGER PARTIALLY FILLED WITH A METAL FOAM AND ROTATING COAXIALLY

Ahmed Alhusseny[1, 2, *], Ali Turan[1], Adel Nasser[1], and Nabeel Al-zurfi[1, 2]
*Author for correspondence
[1]School of Mechanical, Aerospace, and Civil Engineering,
University of Manchester,
Manchester, M13 9PL,
UK,
[2]Mechanical Engineering Department, College of Engineering, University of Kufa, Najaf, Iraq,
E-mail: ahmed.alhusseny@manchester.ac.uk

ABSTRACT

In order to enhance the amount of heat transported in a double-pipe heat exchanger, a compound enhancement is proposed herein incorporating both active and passive methods. The first one is through introducing secondary flows in the vicinity of the conducting surface using metal foam guiding vanes, which are fixed obliquely and rotating coaxially to trap fluid particles while rotation and then force them to flow over the conducting surface. The other is via covering the conducting surface between the two pipes with a metal foam layer to improve the heat conductance across it. This proposal is examined numerically by studying the three-dimensional, steady, incompressible, and laminar convective fluid flow in a counter-flow double-pipe heat exchanger partially filled with high porosity metal foam and rotating in a coaxial-mode. In regards to the influence of rotation, both the centrifugal buoyancy and Coriolis forces are considered in the current study. The generalised model is used to mathematically simulate the momentum equations in the porous regions employing the Boussinesq approximation for the density variation. Moreover, thermal dispersion has been taken into account with considering that fluid and solid phases are in a local thermal non-equilibrium. Computations are performed for a range of design parameters influencing the performance achieved such as the operating conditions and the configuration of the guiding vanes utilised. The results are presented by means of the heat exchanger effectiveness, pressure drop, and the overall system performance. The current proposal has proved its potential to enhance the heat transported considerably with saving significant amount of the pumping power required compared to the corresponding heat exchangers, which are fully filled with metal foam. Also, the data obtained reveal an obvious impact of the design parameters inspected on both the heat exchanged and the pressure loss; and hence, the overall performance obtained. Although the heat exchanger effectiveness can be improved considerably by manipulating the design factors, care must be taken to avoid unjustified expenses resulted from potential augmentation in pressure drop.

NOMENCLATURE

a_{sf}	[1/m]	Solid-fluid interfacial specific surface area
c_p	[J/ kg·K]	Fluid specific heat
D_h	[m]	Hydraulic diameter
F	[-]	Inertial coefficient
Gr_Ω	[-]	Rotational Grashof number, $Gr_\Omega = \Omega^2 \cdot R \cdot \beta \cdot \Delta T_c \cdot D_h^3 / \nu^2$
h_{sf}	[W/m^2·K]	Solid-fluid interfacial heat transfer coefficient
k	[W/m·K]	Thermal conductivity
K	[m^2]	Permeability
L	[m]	Length of heat exchange section
OSP	[-]	Overall system performance
p	[Pa/m]	Pressure
PP	[W]	Pumping power
Q	[W]	Heat transfer rate
r	[m]	Radial distance from the axis of rotation
Re	[-]	Reynolds number, $Re = \rho \cdot u_{in} \cdot D_h / \mu$
Ro	[-]	Rotation number, $Ro = \Omega \cdot D_h / u_{in}$
T	[K]	Temperature
$\mathbf{v}$	[m/s]	Dimensional velocity vector
u, v, w	[m/s]	Cartesian axis direction
$\mathbf{x}$	[m]	Dimensional position vector
x, y, z	[m]	Dimensional coordinates

Special characters

ϕ	[-]	Porosity
ε	[-]	Heat exchanger effectiveness
ω	[PPI]	Pore Density
ρ	[kg/m^3]	Density
Ψ	[-]	Dimensionless axial vorticity
μ	[Pa·s]	Dynamic viscosity
Ω	[rpm]	Rotational speed
θ	[-]	Dimensionless temperature, $\theta = (T - T_{c,1}) / (T_{h,1} - T_{c,1})$

Subscripts

c, h	Cold, hot
d	Dispersive
f, s	Fluid, solid
fe, se	Fluid effective, solid effective
in	Inlet
sf	Solid-to-fluid
w	Wall
1, 2	Inlet to, Exit from

INTRODUCTION

Improving the performance of power generation plants while reducing the environmental damage caused by using fossil fuels remains of great concern. To achieve a high thermal efficiency in power generation systems, heat recirculation is

applied between the cold intake and hot exhausts to recover a part of its thermal energy instead of releasing it directly to the environment [1]. Heat recirculation is usually accomplished by means of two alternatives. Either a recuperator or regenerator depending on whether the heat exchange takes place directly via a thermally conductive surface separating the two streams or through an intermediate storage medium exposed to them alternately, respectively, [2].

Among the various arrangement of recuperators available in industry and practical applications, the simplest one is the double-pipe heat exchanger. This arrangement is widely utilised in practical applications, and hence, has been the focus of plenty of studies recently. In the light of economic considerations, many efforts have been made to construct cheaper and smaller but more effective heat exchangers.

Among these investigations, some have been dedicated to renew the boundary layer developing over the heat exchange surface, and hence, enhance the amount of heat transported. For example, it was found that placing propellers inside the inner tube leads to enhance the heat exchanged by up to **250%** and a further enhancement can be achieved by increasing Reynolds number and/or the number of propellers used [3]. Another passive way is to place a strip turbulator twisted in certain angles to touch the inside wall of the inner pipe [4], where heat transfer rate can be improved by **100%** or more through increasing the pitch length.

Also, the effectiveness of double-pipe heat exchangers can be improved considerably by either covering the conducting surface with a porous layer [5] or through attaching porous structures to this surface [6],[7].

Due to their ability to meet the highly thermal demands with no excessive loss in pressure, open-cell metal foams have been utilised in heat exchangers [8], [9] besides internal cooling of both turbine blades [10] and the rotor windings of high-capacity electrical generators [11], [12], and [13]. Thus, it is not surprising to use them recently in double-pipe heat exchangers [14] and [15], where a substantial enhancement in the heat transfer performance has been acquired.

The current paper is dedicated to present a proposal to improve the performance of a double-pipe heat exchanger. A compound enhancement method is suggested including both passive, i.e. using metal foam structures, and active technique, by subjecting the system to a coaxial rotation. The worth gained from using such configuration is checked numerically taking into account the potential losses due to the increase in pressure drop.

MATHEMATICAL FORMULATION

Two steady, incompressible, laminar, and counter-flowing streams are carried in a heat exchanger rotating coaxially and comprised of two annular pipes separated with a **2mm** stainless steel heat conducting surface, as shown in **Figure 1**.

Both sides of the conducting surface are covered with a **2mm** layer of metal foam, while the space left in both annuli is partially occupied with guiding vanes made of metal foam and fixed obliquely to trap fluid particles while rotation and then force them to flow over the conducting surface. The total length of the heat exchange section is **400mm**, while the internal and external diameters of the inner annular tube are $\mathbf{D_i=20}$ and $\mathbf{D_1=40mm}$, respectively, and their values for the outer pipe are $\mathbf{D_2=44}$ and $\mathbf{D_o=64mm}$, respectively. Also, both channels are further extended to establish the condition of fully developed convective flow at the outlet of each one of them, while both the flow and temperature fields are assumed to be uniform at the inlet sections. All lateral walls of the heat exchanger are impermeable and thermally insulated, while heat is only allowed to transport between the two streams via the conducting surface separating them.

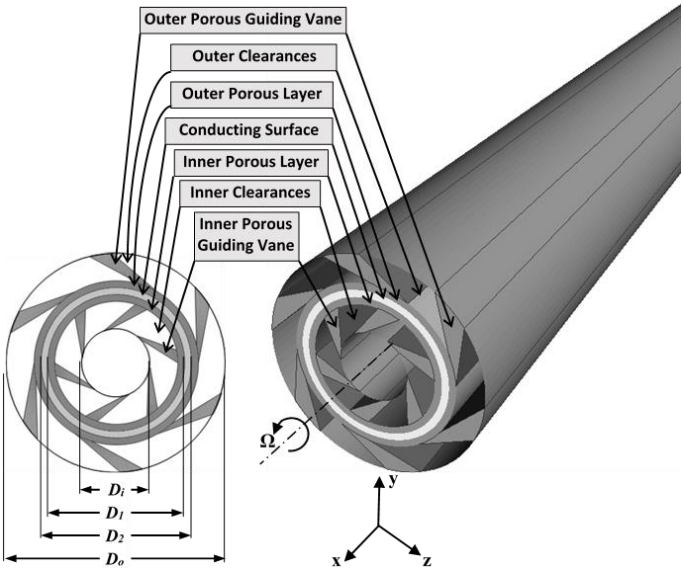

Figure 1 Geometrical shape of the studied problem

The porous material is considered isotropic, homogeneous, and rigid metal foam of high porosity $\phi \geq 0.89$. The generalised model is employed to simulate the momentum equations considering both the solid and fluid phases to be in local thermal non-equilibrium with each other. Both fluid and solid properties are assumed to be constant everywhere except the fluid density in the centrifugal buoyancy term, which varies according to the Boussinesq approximation.

Thus, the dimensional forms of conservation equations of mass, momentum, and energy for both fluid and solid-phase as well as the conducting surface are:

$$\nabla \cdot \mathbf{v} = 0 \tag{1}$$

$$\begin{aligned} \frac{\rho_f}{\phi^2}(\mathbf{v}\cdot\nabla)\mathbf{v} = &-\nabla p_r + \frac{\mu}{\phi}\nabla^2\mathbf{v} - \frac{2\rho_f\,\Omega}{\phi}e_\Omega \times \mathbf{v} \\ &+ \left(\rho_f - \rho_0\right)\Omega^2 e_\Omega \times (e_\Omega \times \mathbf{x}) \\ &- \gamma\left(\frac{\mu}{K}\mathbf{v} + \rho_f \frac{F}{\sqrt{K}}|\mathbf{v}|\,\mathbf{v}\right) \end{aligned} \tag{2}$$

$$\begin{aligned} \rho_f\, c_p(\mathbf{v}\cdot\nabla)T_f = &(1-\gamma)k_f\nabla^2 T_f \\ &+ \gamma\left[(k_{fe}+k_d)\nabla^2 T_f + a_{sf}h_{sf}(T_s - T_f)\right] \end{aligned} \tag{3}$$

$$0 = k_{se}\nabla^2 T_s + a_{sf}h_{sf}(T_f - T_s) \tag{4}$$

$$0 = k_w \nabla^2 T_w \tag{5}$$

In Eqs.[(2), (3)], γ is a distinguishing parameter equals to either zero or one depending on whether the flow takes place in the hollow or porous region, respectively; while the medium porosity ϕ equals to one just in the hollow region. Also, $p_r = p - \rho_0 \Omega^2 (e_\Omega \times x) \cdot (e_\Omega \times x)/2$ is the reduced pressure generalised to include the constant components of the centrifugal terms, while K and F represent the permeability and inertial coefficient of the metal foam, respectively, where their values are computed according to the model proposed by Calmidi [16] as:

$$K = 0.00073\, d_p^2 (1-\phi)^{-0.224} \left(\frac{d_f}{d_p} \right)^{-1.11} \tag{6}$$

$$F = 0.00212\, (1-\phi)^{-0.132} \left(\frac{d_f}{d_p} \right)^{-1.63} \tag{7}$$

In addition, k_{fe} and k_{se} are the effective thermal conductivity of fluid and solid phase, respectively. Their values are computed using the model developed by Boomsma and Poulikakos [17] and corrected by them [18]. The dispersion conductivity k_d, which is assumed to be isotropic, is determined based on the model presented by Hunt and Tien [19]:

$$k_d = C_d \rho c_p u \sqrt{K} \tag{8}$$

Where C_d is the coefficient of thermal dispersion and its value was found to be **0.06** as proposed by Calmidi and Mahajan [20]. Finally, a_{sf} and h_{sf} are the solid-fluid interfacial specific surface area and heat transfer coefficient and can be determined using the model suggested by Calmidi and Mahajan [20]. However, the h_{sf} value is estimated using the model proposed by Lu et al. [21] rather than the one presented by Calmidi and Mahajan [20] due to its generality in not only relying on foam porosity and fiber diameter, but being a function to the pore flow regime as well.

Although the governing equations of fluid flow and heat transport either within the metal foam or in the clearances zones are not coupled with each other, they are linked together through interface surfaces separating them. So, Eqs.[(1) – (4)] need to be closed by means of interfacial coupling conditions, where continuity of velocity, shear stress, fluid temperature, and heat flux along the fluid–solid interfaces shown in **Figure 2** must be ensured to get meaningful physics [13]. To this end, boundary conditions proposed by Ochoa-Tapia and Whitaker [22] for the fluid-solid interface are used with taking the thermal dispersion into account as:

$$\left.\begin{aligned}
&\mathbf{v}\big|_{\mathrm{int}_H}^{n} = \mathbf{v}\big|_{\mathrm{int}_P}^{n} \\
&\mu_f \nabla \mathbf{v}\big|_{\mathrm{int}_H}^{n} = \frac{\mu_f}{\phi} \nabla \mathbf{v}\Big|_{\mathrm{int}_P}^{n} \\
&T_f\big|_{\mathrm{int}_H}^{n} = T_f\big|_{\mathrm{int}_P}^{n} \\
&k_f \nabla T_f\big|_{\mathrm{int}_H}^{n} = \left((k_{fe} + k_d) \nabla T_f + k_{se} \nabla T_s \right)\big|_{\mathrm{int}_P}^{n} \\
&k_{se} \nabla T_s\big|_{\mathrm{int}_P}^{n} = h_{sf} \left(T_s\big|_{\mathrm{int}_P}^{n} - T_f\big|_{\mathrm{int}_H}^{n} \right)
\end{aligned}\right\} \tag{9}$$

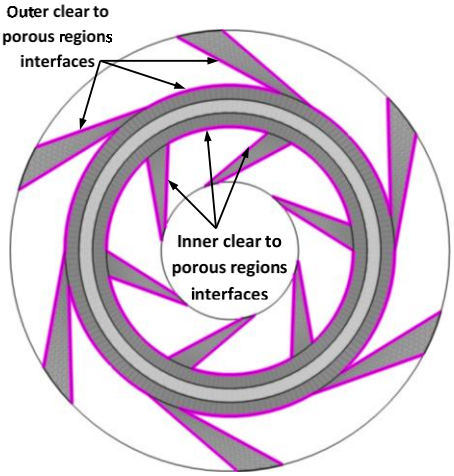

Figure 2 Interfaces between the clear and the porous regions

As the flow is assumed to be thermally and hydrodynamically developing, the velocity and temperature profiles are considered uniform at the channel inlet. Moreover, the no-slip condition is applied at the walls in addition to assuming that the heat transported to/from the conducting surface is divided between the fluid and solid phases depending on their effective thermal conductivities and temperature gradients at the channel walls. Hence, the dimensionless forms of boundary conditions employed to solve the aforementioned governing equations are:

$$\left.\begin{aligned}
&at\ \ x = 0; \\
&\begin{cases}
D_i < D < D_1: & u = u_{c,in},\ v = w = 0,\ T_f = T_s = T_{c,in} \\
D_1 < D < D_2: & \dfrac{\partial T_w}{\partial x} = 0 \\
D_2 < D < D_o: & \dfrac{\partial u}{\partial x} = \dfrac{\partial v}{\partial x} = \dfrac{\partial w}{\partial x} = \dfrac{\partial T_f}{\partial x} = \dfrac{\partial T_s}{\partial x} = 0
\end{cases} \\
&at\ \ x = L; \\
&\begin{cases}
D_i < D < D_1: & \dfrac{\partial u}{\partial x} = \dfrac{\partial v}{\partial x} = \dfrac{\partial w}{\partial x} = \dfrac{\partial T_f}{\partial x} = \dfrac{\partial T_s}{\partial x} = 0 \\
D_1 < D < D_2: & \dfrac{\partial T_w}{\partial x} = 0 \\
D_2 < D < D_o: & u = u_{h,in},\ v = w = 0,\ T_f = T_s = T_{h,in}
\end{cases} \\
&at\ \ 0 < x < L; \\
&\begin{cases}
D = D_i: & u = v = w = 0,\ \dfrac{\partial T_f}{\partial \mathbf{x}_n} = \dfrac{\partial T_s}{\partial \mathbf{x}_n} = 0 \\
D = D_1; D_2: & u = v = w = 0,\ k_{se} \dfrac{\partial T_s}{\partial \mathbf{x}_n} + (k_{fe} + k_d) \dfrac{\partial T_f}{\partial \mathbf{x}_n} = k_w \dfrac{\partial T_w}{\partial \mathbf{x}_n} \\
D = D_o: & u = v = w = 0,\ \dfrac{\partial T_f}{\partial \mathbf{x}_n} = \dfrac{\partial T_s}{\partial \mathbf{x}_n} = 0
\end{cases}
\end{aligned}\right\} \tag{10}$$

SOLUTION PROCEDURE

The governing equations mentioned earlier are discretised using the finite volume method. The second-order differencing scheme is employed to represent the convection terms of the discretised governing equations, while the problem of pressure–velocity coupling is resolved using *SIMPLE* algorithm.

A structured grid formed of hexahedral elements was built using Pointwise software, where the stationary clear regions are linked to the rotating porous regions through four interface surfaces as shown in **Figure 3**. Steep gradients expected at the boundaries including the walls and the interfaces are captured by refining the mesh at these regions. Grid dependency was checked by examining four sets of grid including the rotating porous and stationary non-porous regions (**914,620**, **1,222,420**, **1,541,380**, and **1,838,020**) at $Re_{inner}=Re_{outer}=2000$, $\Omega=500rpm$, $k_s=k_w$, $\phi=0.9$, and $\omega=10PPI$, where the fluid temperature profile along the horizontal mid-plane at **z=0** core for two longitudinal locations, as shown in **Figure 4**. It is noticed that the deviation in data obtained becomes marginal between the third and fourth set of the grid and thereafter. Accordingly, the mesh size of (**1,541,380**) can be considered sufficient for the accuracy of the current study.

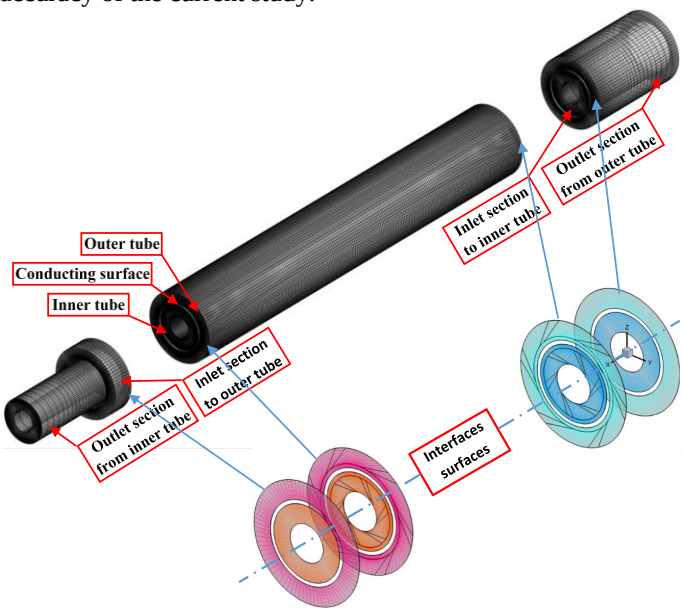

Figure 3 The used grid with the interfaces linking the stationary clear to the rotating porous regions

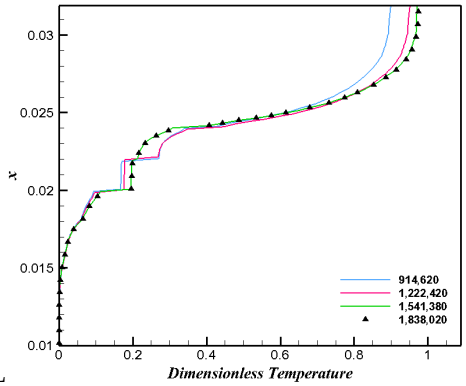

a) x=1%L

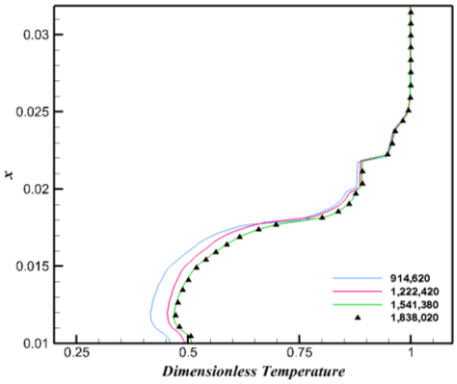

b) x=99%L

Figure 4 Grid dependency of temperature profiles Continued

The "STAR CCM+" commercial CFD code is utilised to simulate the current problem. However, this software does not support using what known as "the local thermal non-equilibrium model" to track the solid-to-fluid interstitial heat transport within the porous regions. To overcome this drawback, the porous region was duplicated into two identical zones representing the solid and fluid phase individually and then heat can be allowed to transfer between the two phases and tracked by creating a heat exchanger interface there. Under-relaxation technique is used in order to avoid divergence during the iterative process, where under-relaxation factors of about (**0.3**–**0.99**) are used for the dependent variables. Convergence is measured in terms of the maximum change in the difference between the heat transported from the outer stream to the conducting surface and that transferred from the conducting surface to the inner stream during any iteration, where the maximum change allowed for convergence check is 10^{-5}.

Due to the lack of experiments conducted on heat and fluid flow in double-pipe heat exchangers filled with metal foam, the currently computed data were validated with the numerical data presented by Xu et al. [14] for a stationary heat exchanger. The profiles of dimensionless axial velocity at the exit section of each pipe were compared with the corresponding data from the above mentioned study as shown in **Figure 5**. Overall, the currently computed results are in excellent agreement with numerical data presented in the above mentioned study.

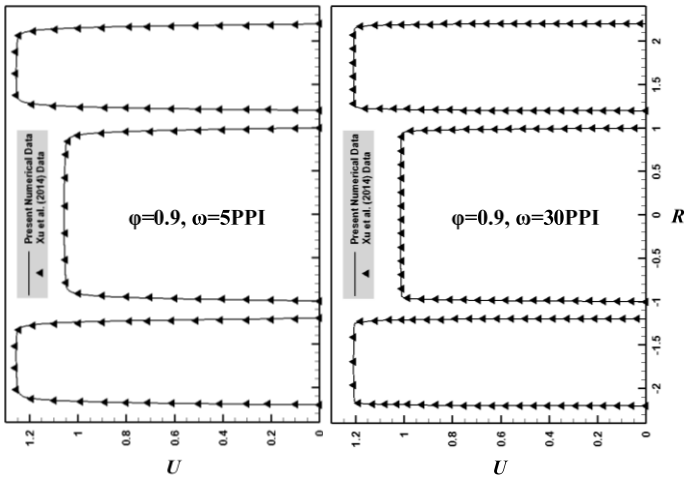

Figure 5 Velocity profile at the exit sections of a heat exchanger fully filled with metal foam at $Re_{inner}=Re_{outer}=1000$

RESULTS

The efficiency of heat exchange process is mainly measured in terms of two key design parameters. The first is the effectiveness, which can be computed as:

$$\varepsilon = \frac{Q_c}{Q_{\max}} = \frac{Q_h}{Q_{\max}} \tag{11}$$

Where;

$$\left.\begin{aligned} Q_c &= C_c(T_{c,2} - T_{c,1}) \\ Q_h &= C_h(T_{h,1} - T_{c,1}) \\ Q_{\max} &= C_{\min}(T_{h,1} - T_{c,1}) \end{aligned}\right\} \tag{12}$$

Where $\mathbf{C_{min}}$ is the smaller of the hot ($\mathbf{C_h}$) and the cold ($\mathbf{C_c}$) fluid-phase heat-capacity rates.

The other key parameter in assessing the overall performance is the total pressure loss $\mathbf{\Delta P_t}$ occurring across the heat exchanger, which indicates the pumping power required as:

$$PP_t = PP_c + PP_h = \dot{V}_c \Delta p_c + \dot{V}_h \Delta p_h = \left.\frac{\dot{m}}{\rho}\right|_c \Delta p_c + \left.\frac{\dot{m}}{\rho}\right|_h \Delta p_h \tag{13}$$

To examine the practical worth of using specific design or flow characteristics, a performance measure called the overall system performance ***OSP*** is introduced as the ratio of the heat transported to the pumping power required. So, the higher the ***OSP***, the better the overall performance achieved.

The obtained results are presented for various range of rotational speed (**0≤ Ω ≤500rpm**) and clearance-to-vane size ratio (**0≤*S*≤4**), while fixed values are considered for the porosity ϕ**=0.9**, pore density ω**=10PPI**, solid-phase to wall thermal conductivity ratio k_s/k_w**=1**, Prandtl number ***Pr*=0.7**, inlet Reynolds number for the inner and outer pipe Re_{inner}**=** Re_{outer}**=2000**, and the inlet temperature to the inner and outer pipe $T_{c,in}$**=20°C** and $T_{h,in}$**=50°C**, respectively.

Rotation effects on the development of flow field and heat transfer are illustrated in **Figure 6** for various axial locations at ***S*=2**, and **Ω=500rpm**. When the two counter-flowing streams enter to the rotating heat exchange part, influence of body forces induced by rotation starts to appear, i.e. Coriolis and centrifugal forces, resulting in forming transverse vortices and reorganising the flow patterns in a quite different way from the classical flow behavior. As a result of Coriolis forces, a main counter-to-rotation vortex is created at the entrance of each of the inner and outer pipe, i.e. **x=1%L** and **99%L**, respectively. Thereafter, this vortex induces further smaller ones trapped in the clear regions due to the rotating vanes, which act as a semi-buffer that forces the fluid particles to swirl and then flow back over the conducting surface through the porous layer covering it. Consequently, the boundary layer in the vicinity of the conducting surface becomes thinner, which leads to reactivate the heat exchange surface continually. As the fluid flows downstream, however, the secondary flows are alleviated gradually along the main flow path until they almost vanish close to the exit of each pipe. This is attributed to the negligibly small vorticity generation close to the fully-developed region, as inferred by Soong and Yan [23].

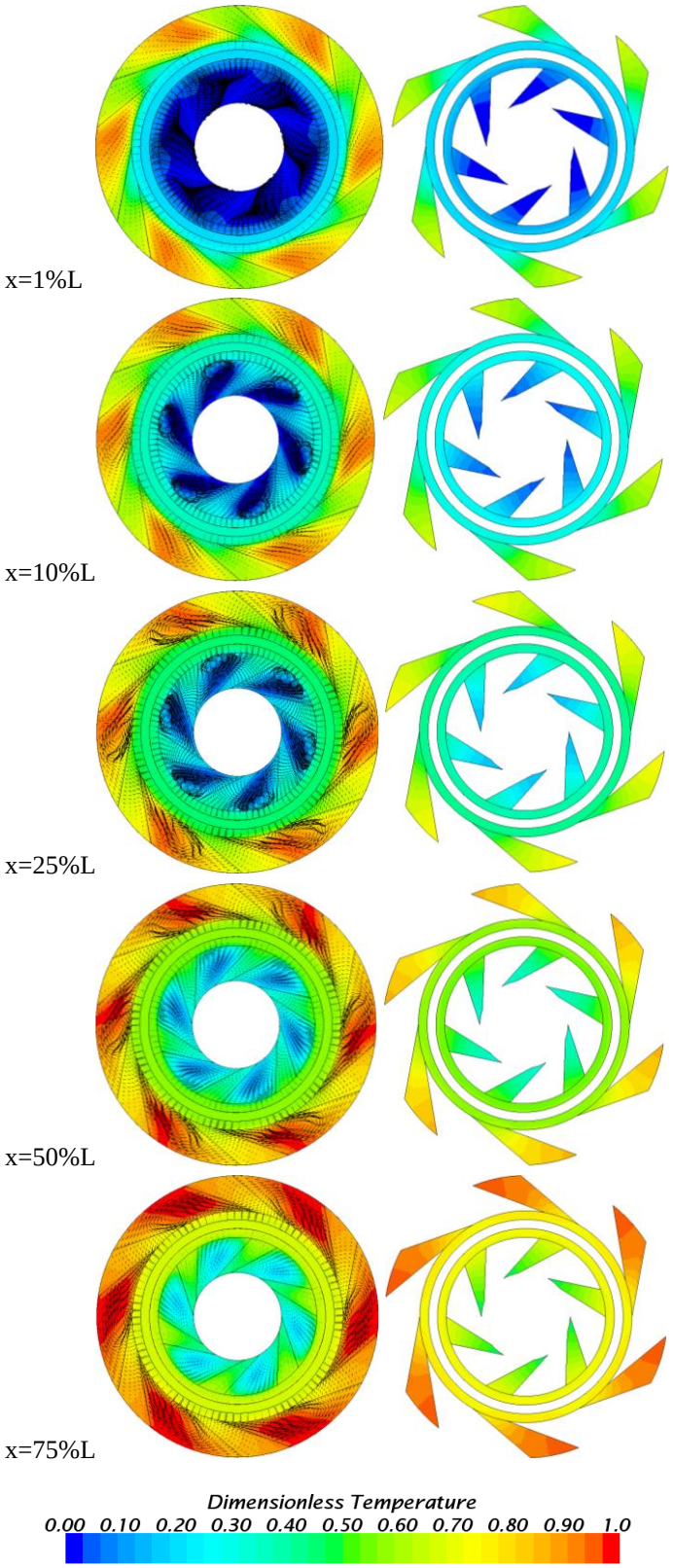

Figure 6 Transverse velocity vectors in rotating frame and dimensionless temperature of fluid (left) and solid-phase (right)

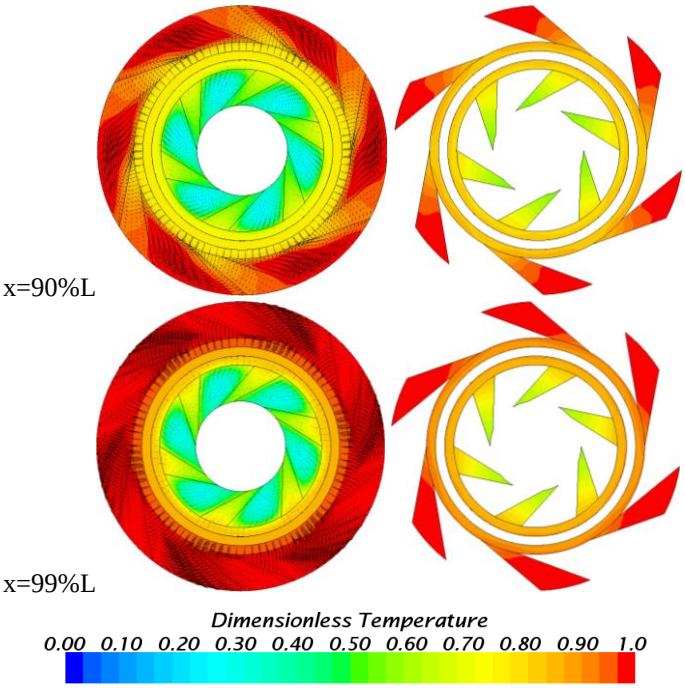

Figure 6 Continued

To justify this phenomenon, it is better to look closely at the dimensionless equation of axial vorticity transport presented earlier by Soong and Yan [23] but modified to take into account the foam presence as:

$$\frac{1}{\phi^2}\left[\left(U\frac{\partial\Psi}{\partial X}+V\frac{\partial\Psi}{\partial Y}+W\frac{\partial\Psi}{\partial Z}\right)+\Psi\frac{\partial U}{\partial X}+\left(\frac{\partial U}{\partial Y}\frac{\partial W}{\partial X}-\frac{\partial U}{\partial Z}\frac{\partial V}{\partial X}\right)\right]$$
$$=\frac{1}{\phi\,\mathrm{Re}}\left(\frac{\partial^2\Psi}{\partial X^2}+\frac{\partial^2\Psi}{\partial Y^2}+\frac{\partial^2\Psi}{\partial Z^2}\right)-\gamma\left(\frac{1}{Da\,\mathrm{Re}}+\frac{F|\mathbf{V}|}{\sqrt{Da}}\right)\Psi \qquad (14)$$
$$+\frac{2Ro}{\phi}\frac{\partial U}{\partial X}+\frac{Gr_\Omega}{\mathrm{Re}^2}\left(Y\frac{\partial\theta_f}{\partial Z}-Z\frac{\partial\theta_f}{\partial Y}\right)$$

Where **Ψ** is the axial vorticity and is defined as:

$$\Psi=\frac{\partial W}{\partial Y}-\frac{\partial V}{\partial Z} \qquad (15)$$

On the right side of Eq.(14), the second term refers to the vorticity dissipation due to porous resistance, while the last two ones stand for the vorticity generation terms by Coriolis influence and centrifugal buoyancy, respectively. As the axial velocity gradient is steep at the entrance regions, which in turn contributes effectively in the vorticity generation due to Coriolis effects; the secondary flows are very strong there. More downstream, however, velocity gradients start to decrease as an outcome of flow development, and hence, the decreasing Coriolis generation term cannot make up the dissipation occurred in vorticity due to the foam and viscous resistance. Thus, secondary vortices are alleviated gradually until they almost fade away at the fully developed region, where the axial gradients of velocity components become zero.

To explain the effects of rotation level on the flow and heat transfer patterns, the three-dimensional evolution of streamlines based on the fluid-phase temperature are plotted at ***S*=2** and ***Re**=1** for various rotation levels as shown in **Figure 7**. It is observed that increasing the rotation rate enhances the strength of transverse vortices, and hence, reactivates the boundary layer over the heat exchange surface.

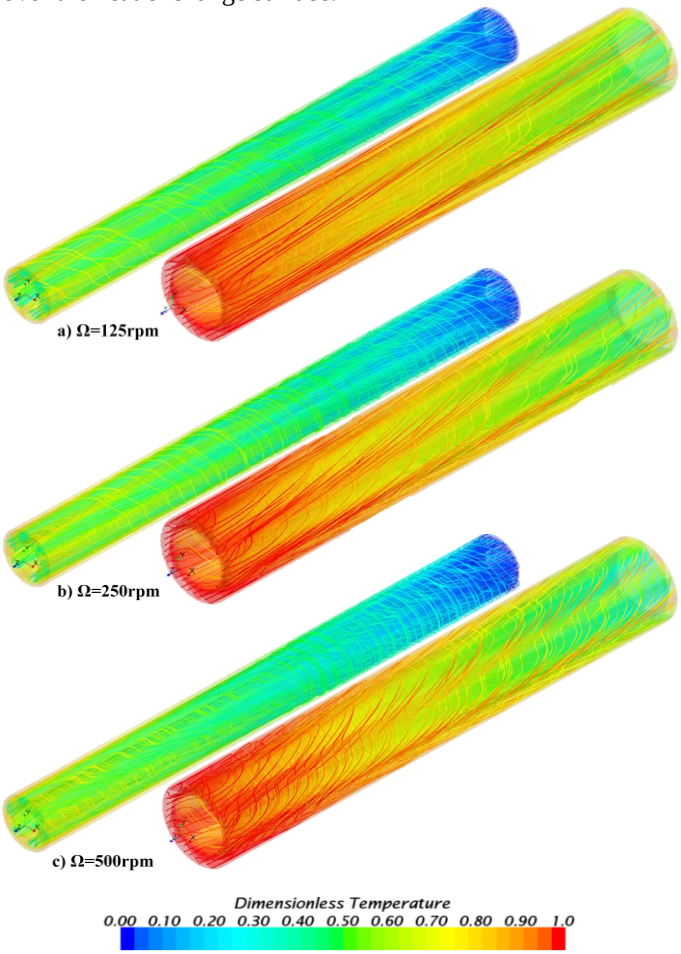

Figure 7 Fluid-phase temperature streamlines at various rotational speed along the inner- (left) and outer-pipe (right)

For further clarification, **Figure 8** shows the development of transverse velocity vectors and fluid temperature contours for two rotational speeds **Ω=125** and **250rpm**, while their patterns at **Ω=500rpm** have already been illustrated in **Figure 6**. In general, the stronger the rotational speed is applied, the better the heat exchange is achieved. Moreover, it is observed that secondary flows in the inner part are enhanced with increasing the rotation rate and sustained for a further downstream as a result of the increase in vorticity generation by Coriolis influence. The secondary vortices in the outer pipe, in contrast, look slightly weaker when the rotation is enhanced. This can be justified by looking closely at Eq.(14), where the higher temperature differences found in the case of lower rotational speeds result in a stronger vorticity generation due to centrifugal buoyancy and vice versa. Hence, this extra bonus in vorticity generation leads to make up or neutralise the dissipation along the flow path in the outer pipe.

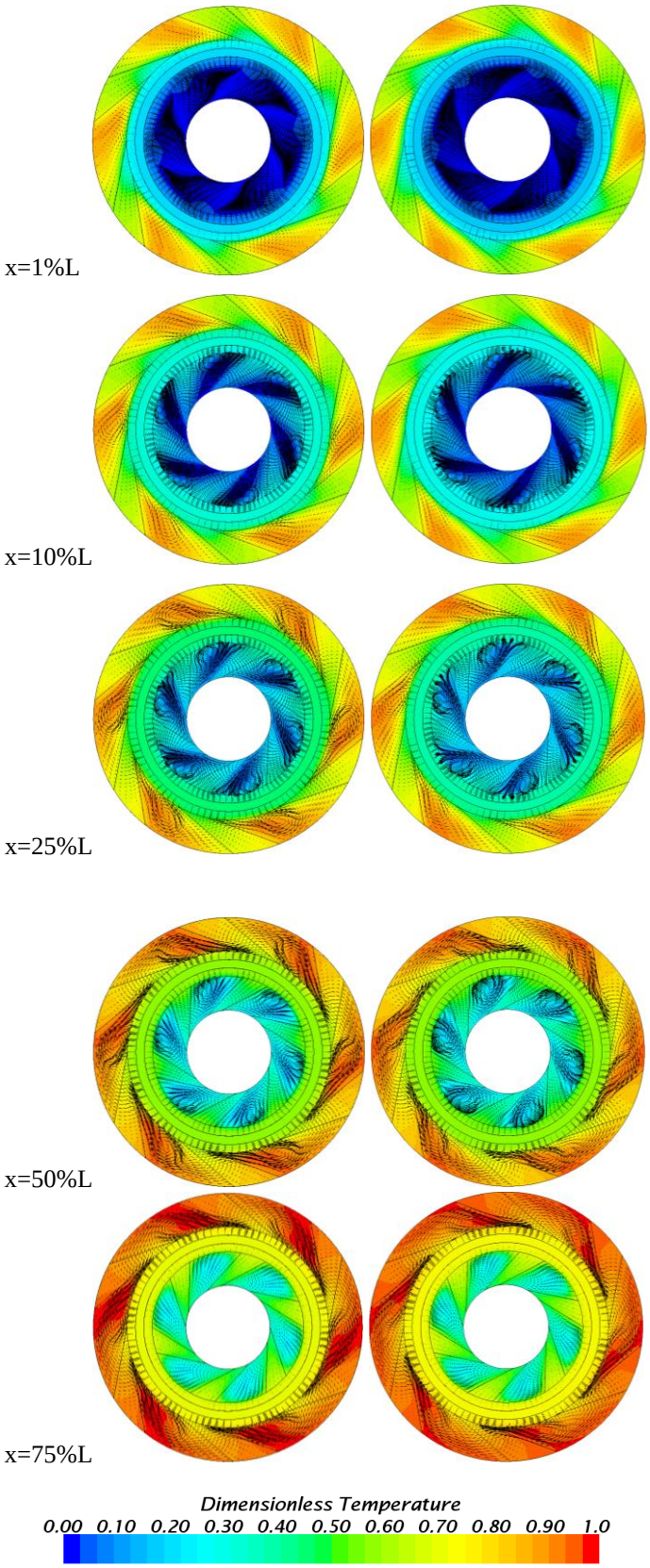

Figure 8 Transverse velocity vectors and dimensionless fluid temperature at Ω=125rpm (left) and Ω=250rpm (right)

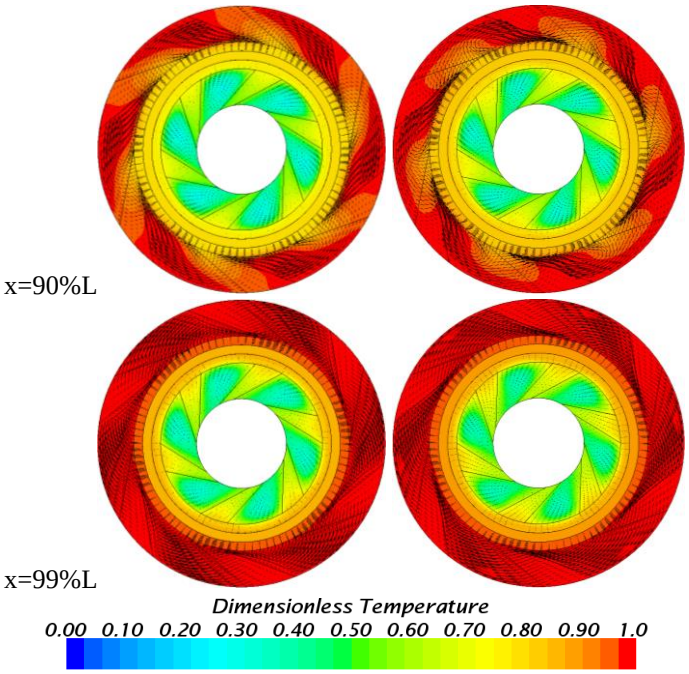

Figure 8 Continued

Generally, this enhancement in heat transfer improves the effectiveness attained as shown in **Figure 9**. However, such this improvement has a drawback, which is the increase in the pressure drop and pumping power required. This is attributed to the augmentation in flow resistance due to enhancing the swirls across the clear and porous regions. In regard to the overall system performance achieved, it is slightly improved at the lower rotation levels, but then starts to deteriorate. This outcome is due to the fact that pressure drop increases marginally at the lower rotation levels, while thereafter its growth becomes considerable causing to augment the pumping power significantly. Overall, the negligibly small pumping power required compared to the amount of heat exchanged makes the overall performance of such heat exchangers incomparable, i.e. $OSP=O(10^2)$.

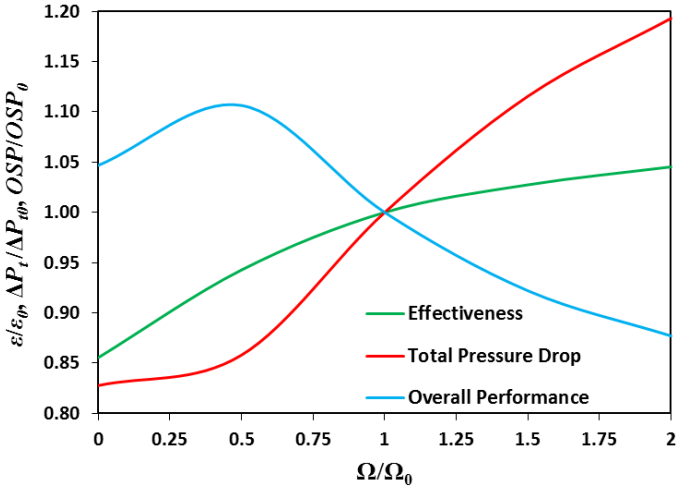

Figure 9 Influence of rotation rate on the effectiveness, total pressure drop, and overall system performance at Ω_0 =250rpm, ε_0 =0.615, ΔP_{t0}=38.24Pa, and OSP_0=353.56

The influence of the hollow ratio, or in other words, the clearances-to-vanes size ratio ***S***, on the transverse velocity vectors and fluid temperature contours is illustrated in **Figure 10** for hollow ratios ***S*=1** and **4**, while their patterns for ***S*=2** have already been presented in **Figure 6**. In general, a less heat exchange is attained when the size of clearances becomes larger. This is due to the reduction in the mass flow across the foam region; and hence, the amount of heat transported is reduced due to the low fluid heat conductance compared to metal foams as shown in **Figure 11**.

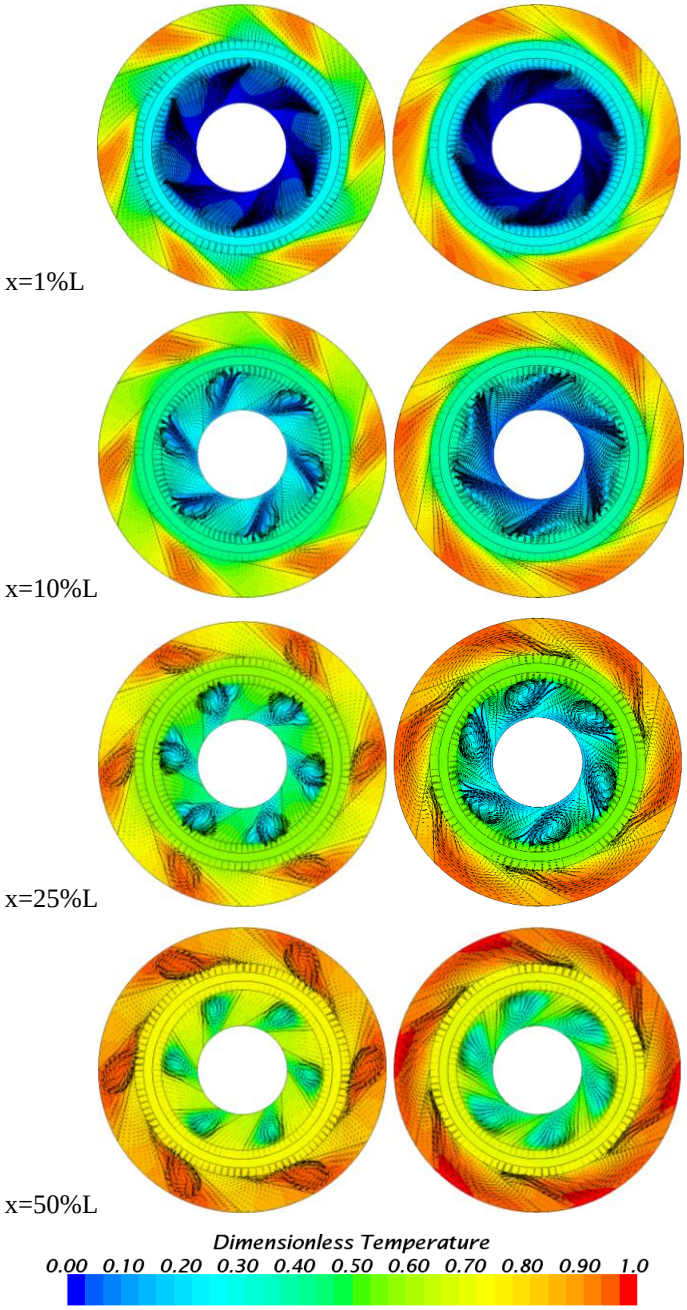

Figure 10 Transverse velocity vectors and dimensionless fluid temperature at Ω=500rpm and S=1 (left) and S=4 (right)

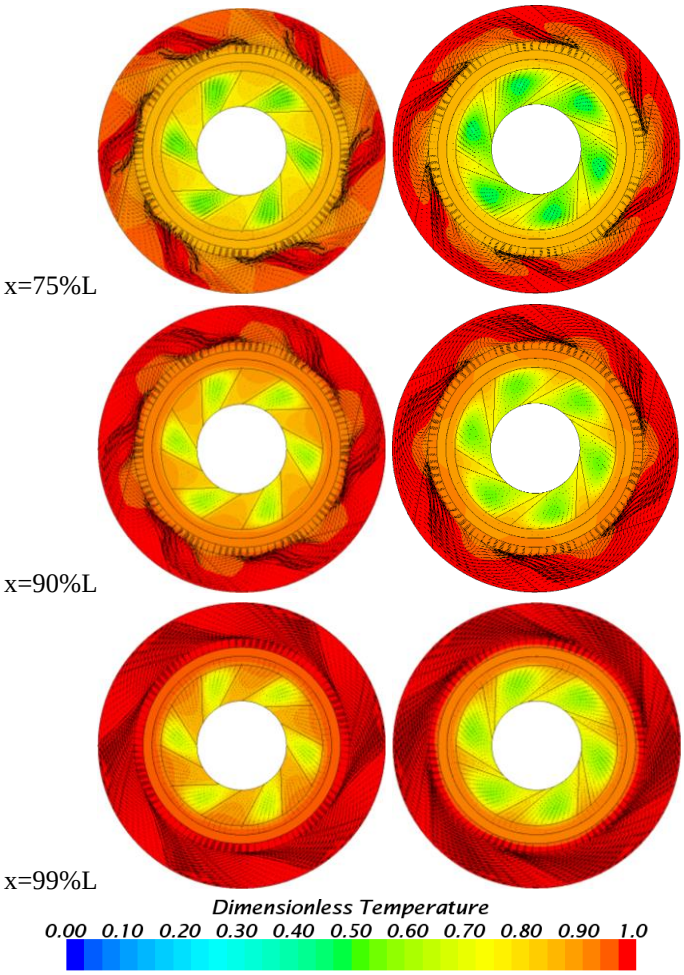

Figure 9 Continued

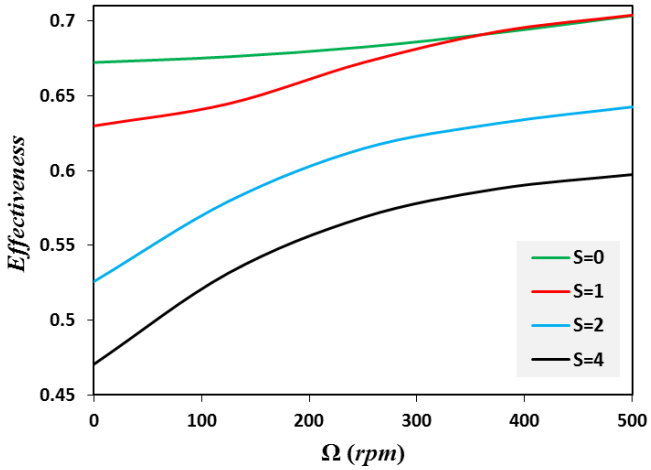

Figure 11 Hollow size influence on the effectiveness achieved

On the other hand, it leads to a significant saving in the pressure drop due to the reduction in the solid matrix volume, which acts as an obstructing or damper to the fluid flowing across it as illustrated in **Figure 12**. However, increasing the rotational speed does not result in the same extent of increase in both heat transfer and pressure drop. Depending on the hollow ratio, it is clear that rotation is less influential at the lower

hollow ratios. This is attributed to the fact that the foam impact dominates rotational effects in both transferring heat and resisting fluid flow within the pipes filled more with metal foams.

In regard to the overall performance attained, **Figure 12** that reducing the size of clearances improves the overall performance considerably as a result of the significant reduction occurred in the pressure drop, where it is obvious that the performance achieved in the heat exchangers semi/fully filled with metal foam, i.e. $S \leq 1$, is negligibly small compared to those having larger clearances, i.e. $S \geq 2$.

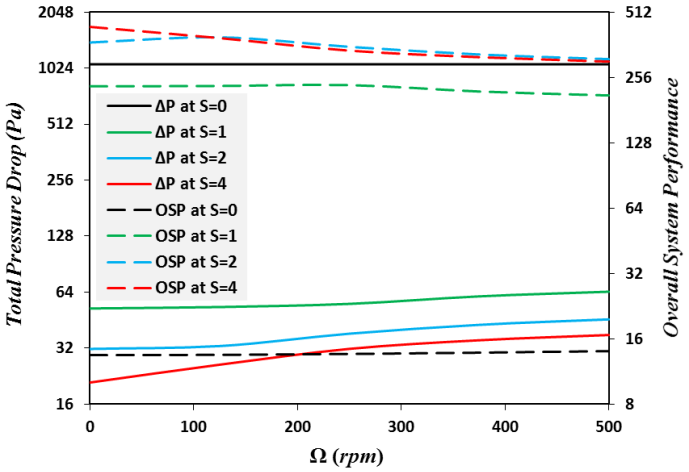

Figure 12 Effects of hollow size on both total pressure drop and the overall performance

CONCLUSION

In the current study, a compound enhancement for the heat transported in a double-pipe heat exchanger is proposed through utilising both active and passive methods. The first is to introduce secondary vortices in the vicinity of the conducting surface using metal foam guiding vanes. The role of these obliquely fixed vanes is to trap fluid particles while rotation and then force them to flow over the conducting surface. The other is via covering the conducting surface between the two pipes with a metal foam layer to improve the heat conductance across it.

This proposal is examined numerically by studying the three-dimensional, steady, incompressible, and laminar convective fluid flow in a counter-flow double-pipe heat exchanger partially filled with high porosity metal foam and rotating in a coaxial-mode. Computations are performed for a range of design parameters influencing the performance achieved such as the rotation strength and the size of the guiding vanes utilised.

The current proposal has proved its potential to enhance the heat transported considerably with saving significant amount of the pumping power required compared to the corresponding heat exchangers, which are fully filled with metal foam. Also, the data obtained reveal an obvious impact of the design parameters inspected on both the heat exchanged and the pressure loss; and hence, the overall performance obtained. In general, the heat transfer can be improved considerably by manipulating the design factors, however, care must be taken to avoid unjustified expenses resulted from potential increase in pressure drop.

REFERENCES

[1] Alhusseny A., and Turan A., An effective engineering computational procedure to analyse and design rotary regenerators using a porous media approach, *International Journal of Heat and Mass Transfer*, Vol. 95, pp. 593–605, 2016.

[2] Hewitt G.F., Shires G.L., and Bott T.R., *Process Heat Transfer*. CRC Press Inc., USA., 1994.

[3] Yildiz C., Bíçer Y., and Pehlívan D., Influence of fluid rotation on the heat transfer and pressure drop in double-pipe heat exchangers, *Applied Energy*, Vol. 54, pp. 49–56, 1996.

[4] Yildiz C., Bíçer Y., and Pehlivan D., Effect of twisted strips on heat transfer and pressure drop in heat exchangers, *Energy Conversion and Management*, Vol. 39, pp. 331–336, 1998.

[5] Alkam M.K., and Al-Nimr M.A., Improving the performance of double-pipe heat exchangers by using porous substrates, *International Journal of Heat and Mass Transfer*, Vol. 42, pp. 3609–3618, 1999.

[6] Targui N., and Kahalerras H., Analysis of fluid flow and heat transfer in a double pipe heat exchanger with porous structures, *Energy Conversion and Management*, Vol. 49, pp. 3217–3229, 2008.

[7] Targui N., and Kahalerras H., Analysis of a double pipe heat exchanger performance by use of porous baffles and pulsating flow, *Energy Conversion and Management*, Vol. 76, pp. 43–54, 2013.

[8] Boomsma K., Poulikakos D., and Zwick F., Metal foams as compact high performance heat exchangers, *Mechanics of Materials*, Vol. 35, pp. 1161–1176, 2003.

[9] Mahjoob S., and Vafai K., A synthesis of fluid and thermal transport models for metal foam heat exchangers, *International Journal of Heat and Mass Transfer*, Vol. 51, pp. 3701–3711, 2008.

[10] Jeng T.-M., Tzeng S.-C., and Xu R., Experimental study of heat transfer characteristics in a 180-deg round turned channel with discrete aluminum-foam blocks, *International Journal of Heat and Mass Transfer*, Vol. 71, pp. 133–141, 2014.

[11] Alhusseny A., and Turan A., Effects of centrifugal buoyancy on developing convective laminar flow in a square channel occupied with a high porosity fibrous medium, *International Journal of Heat and Mass Transfer*, Vol. 82, pp. 335–347, 2015.

[12] Alhusseny A., Turan A., Nasser A., and Hidri F., Hydrodynamically and thermally developing flow in a rectangular channel filled with a high porosity fiber and rotating about a parallel axis, *International Communications in Heat and Mass Transfer*, Vol. 67, pp. 114–123, 2015.

[13] Alhusseny A., Turan A., and Nasser A., Developing convective flow in a square channel partially filled with a high porosity metal foam and rotating in a parallel-mode, *International Journal of Heat and Mass Transfer*, Vol. 90, pp. 578–590, 2015.

[14] Xu H.J., Qu Z.G., and Tao W.Q., Numerical investigation on self-coupling heat transfer in a counter-flow double-pipe heat exchanger filled with metallic foams, *Applied Thermal Engineering*, Vol. 66, pp. 43–54, 2014.

[15] Chen X., Tavakkoli F., and Vafai K., Analysis and characterization of metal foam-filled double-pipe heat exchangers, *Numerical Heat Transfer, Part A: Applications*, Vol. 68, pp. 1031–1049, 2015.

[16] Calmidi V.V., *Transport Phenomena in High Porosity Metal Foams*, PhD Thesis, University of Colorado, 1998.
[17] Boomsma K., and Poulikakos D., On the effective thermal conductivity of a three- dimensionally structured Fluid-saturated metal foam, *International Journal of Heat and Mass Transfer*, Vol. 44, pp. 827–836, 2001.
[18] Boomsma K., and Poulikakos D., Corrigendum for the paper: K. Boomsma, D. Poulikakos, "On the effective thermal conductivity of a three-dimensionally structured fluid-saturated metal foam" [International Journal of Heat and Mass Transfer, 44 (2001) 827–836], *International Journal of Heat and Mass Transfer*, Vol. 54, pp. 746–748, 2011.
[19] Hunt M.L., and Tien C.L., Effects of thermal dispersion on forced convection in fibrous media, *International Journal of Heat and Mass Transfer*, Vol. 31, pp. 301–309, 1988.
[20] Calmidi V.V., and Mahajan R.L., Forced Convection in High Porosity Metal Foams, *Journal of Heat Transfer*, Vol. 122, pp. 557–565, 2000.
[21] Lu W., Zhao C.Y., and Tassou S.A., Thermal analysis on metal-foam filled heat exchangers. Part I: Metal-foam filled pipes, *International Journal of Heat and Mass Transfer*, Vol. 49, pp. 2751–2761, 2006.
[22] Ochoa-Tapia J.A., and Whitaker S., Heat transfer at the boundary between a porous medium and a homogeneous fluid, *International Journal of Heat and Mass Transfer*, Vol. 40, pp. 2691–2707, 1997.
[23] Soong C.Y., and Yan W.M., Development of secondary flow and convective heat transfer in isothermal/iso-flux rectangular ducts rotating about a parallel axis, *International Journal of Heat and Mass Transfer*, Vol. 42, pp. 497–510, 1999.